Equilibrium partial pressure of CO 2 in Callovian-Oxfordian argillite as a func-tion of relative humidity: experiments and modelling

Arnault Lassin, Nicolas C.M. Marty, Hélène Gailhanou, Benoît Henry, Joachim Trémosa, Catherine Lerouge, Benoît Madé, Scott Altmann, Eric C. Gaucher

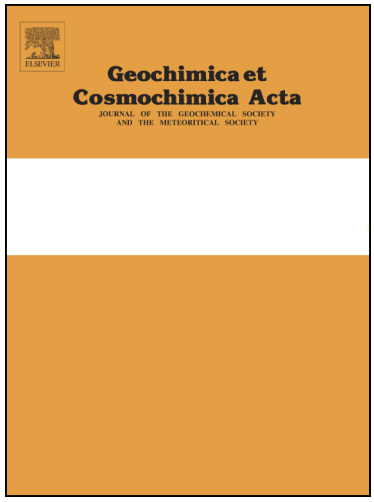

Equilibrium partial pressure of CO_2 in Callovian-Oxfordian argillite as a function of relative humidity: experiments and modelling

Arnault Lassin, Nicolas C.M. Marty, Hélène Gailhanou, Benoît Henry, Joachim Trémosa, Catherine Lerouge, Benoît Madé, Scott Altmann, Eric C. Gaucher

PII: S0016-7037(16)30197-1
DOI: http://dx.doi.org/10.1016/j.gca.2016.04.028
Reference: GCA 9723

To appear in: *Geochimica et Cosmochimica Acta*

Received Date: 19 October 2015
Accepted Date: 18 April 2016

Please cite this article as: Lassin, A., Marty, N.C.M., Gailhanou, H., Henry, B., Trémosa, J., Lerouge, C., Madé, B., Altmann, S., Gaucher, E.C., Equilibrium partial pressure of CO_2 in Callovian-Oxfordian argillite as a function of relative humidity: experiments and modelling, *Geochimica et Cosmochimica Acta* (2016), doi: http://dx.doi.org/10.1016/j.gca.2016.04.028

Equilibrium partial pressure of CO_2 in Callovian-Oxfordian argillite as a function of relative humidity: experiments and modelling

Arnault Lassin[a*], Nicolas C.M. Marty[b], Hélène Gailhanou[b], Benoît Henry[b], Joachim Trémosa[b], Catherine Lerouge[b], Benoît Madé[c], Scott Altmann[c], Eric C. Gaucher[b 1]

a BRGM-ISTO-UMR 7327, 3 av. C. Guillemin, B.P. 36009, Orléans, 45060, France

b BRGM, 3 av. C. Guillemin, B.P. 36009, Orléans, 45060, France

c Andra, 1-7 rue Jean Monnet, Châtenay-Malabry, 92298, France

*** Corresponding author**

Tel.: +33-238-643-025; fax: +33-238-644-797.

E-mail address: a.lassin@brgm.fr (Arnault Lassin)

Postal address: BRGM-ISTO-UMR 7327, 3av. C. Guillemin, B.P. 36009, Orléans, 45060, France

Keywords: pCO_2, Callovian-Oxfordian argillite, capillary systems, relative humidity, isobar/anisobar context, carbon dioxide, geochemical modelling, radioactive waste storage, clay drying, porous media.

[1] Present address: TOTAL, CSTJF, Av. Larribau, 64018, Pau Cedex, France

Abstract

Having previously demonstrated that the mineral assemblage of claystone can impose its pCO_2 under saturated conditions, we here study the effect of rock desaturation, i.e. the evaporation of pore water, on the partial pressure of CO_2 (pCO_2) in Callovian-Oxfordian argillite from the Paris Basin (France). In this new study, which combines experiments at room temperature and geochemical modelling, we examine the primary role of capillary forces on chemical equilibria for relative humidity values ranging between 50% and 100%. In particular we are able, without any fitting parameters, to model the experimental decrease of pCO_2 as a function of decreasing water content in the argillite. This application to a complex natural system not only confirms the theoretical concepts of geochemistry in capillary contexts, but is promising with respect to other systems, both natural (soil, rock) and industrial (ceramics, granular material).

1. Introduction

1.1. PARTIAL PRESSURE OF CO_2 IN SEDIMENTARY ROCK

The pioneering work of Coudrain-Ribstein and Gouze (1993) and Coudrain-Ribstein et al. (1998) showed that, in many confined aquifers, the partial pressure of CO_2 (pCO_2) is determined by equilibrium between calcite, dolomite, and Mg-silicates, which has since been confirmed for clay formations by Gaucher et al. (2006, 2009), Pearson et al. (2011), and Tournassat et al. (2015). This has enabled robust models integrating this key parameter for pore-water chemistry to become available for applications in the framework of research programmes dedicated to radioactive waste disposal in clay formations (Thury and Bossart, 1999; ANDRA, 2005; Landais, 2006; Delay et al., 2007).

The robust models have been used as a basis for reactive-transport modelling involving clay formations hosting nuclear waste (Gaucher et al., 2004; Vieillard et al., 2004; Trotignon et al., 2007; Marty et al., 2009, 2015), and/or for forecasting the mobility of radionuclides (Altmann et al., 2012). However, the effect of rock desaturation (i.e. the evaporation of pore water) on pCO_2 was totally unknown, or at least not considered in these models, despite the fact that desaturation is a major concern in the drifts and galleries of future disposal sites. Further investigations are thus needed to predict the chemical evolution of clay formation pore waters interacting with repository materials under desaturation conditions. This is the subject of the present study, focused on claystone of the Callovian-Oxfordian (COx) argillite formation in the Paris Basin.

1.2. DESATURATION ISSUES

The decreasing water content in rock under desaturation conditions confines water to the smallest pores and generates capillary constraints, i.e. negative pressures in the pore water (Mercury and Tardy, 2001). It is now well known that such conditions change the chemical reactivity of gas-water-rock systems. In particular, the increase of gas

uptake in unsaturated porous media, compared to bulk water, has been observed experimentally (Miachon et al., 2008), studied theoretically (Berkeley and Carey, 2013; Letellier and Turmine, 2013) and/or interpreted from field observations (Henry et al., 1999; Mercury et al., 2004). In addition, recent experiments have shown that capillary constraints also modify the reactivity of simple brine-crystalline salt systems (Bouzid et al., 2011a, b). Such modifications in the chemical reactivity of capillary systems can be more generally described in terms of pressure-induced changes in the thermodynamic properties of water and dissolved species (Zilberbrand, 1999; Mercury et al., 2003; Lassin et al., 2011, 2014). This approach, however, has yet to be applied to a complex geochemical system for which all relevant experimental data are available.

The objective of the present work was to study the effect of claystone desaturation on the equilibrium partial pressure of dissolved CO_2, using an integrated experimental and modelling approach (Lassin et al., 2013). For this we performed outgassing experiments (at room temperature and at different relative humidity [RH] values between 50% and 100%) on COx claystone samples considered to be representative of the rock formation. In this way we obtained a curve of equilibrium partial pressure of dissolved CO_2 as a function of RH and interpreted the resulting data using numerical simulations. Our modelling approach identified and quantified the physical and chemical processes associated with desaturation and their impact on the pCO_2 at equilibrium with the water-rock system, thus enabling us to analyse the impact on the concentration of the main dissolved elements.

2. Theoretical background

2.1. GEOCHEMISTRY OF THE CALLOVIAN-OXFORDIAN FORMATION IN THE CONTEXT OF NUCLEAR WASTE DISPOSAL

The mineral assemblage of the Callovian-Oxfordian (COx) claystone, which traps fluids in its residual porosity, is represented by a dominant detrital fraction of clay minerals, quartz, feldspar and bioclasts, cemented by diagenetic carbonate, sulphide and sulphate minerals (Gaucher et al., 2004; Clauer et al., 2007; Tournassat et al., 2008; Lerouge et al., 2011). The formation fluids are slightly saline waters, with ionic strengths of about 80-100 meq/L (Vinsot et al., 2008), that contain small amounts of dissolved gases. The chemistry of the COx pore water has been studied at ambient temperature (~25 °C) using, in particular, modelling approaches constrained by properties measured on core samples (Gaucher et al., 2006, 2009) and by measurements of pore-water properties collected in boreholes drilled in the Meuse-Haute Marne Underground Rock Laboratory (Vinsot et al., 2008). The resulting predictive model (Gaucher et al., 2009) satisfactorily reproduces the measured *in situ* pore-water composition. It is defined by the thermodynamic equilibrium between the interstitial pore waters, the clay exchanger and the diagenetic minerals (Gaucher et al., 2006, 2009; Tournassat et al., 2015), except for Cl and SO_4 concentrations which are fixed after measured data. The model also indicates that calcite and dolomite, among the most reactive minerals in the claystone, play a major role in controlling the pore-water chemistry. According to the Gibbs phase rule applied to this carbonate system, the aqueous concentrations of Ca and Mg are controlled by equilibrium with calcite and dolomite, respectively, while the aqueous concentration of C and the pH are controlled by alkalinity and the partial pressure of dissolved CO_2 (pCO_2), respectively. But, when monitored *in situ*, the pCO_2 measurements are not sufficiently accurate for constraining the carbonate system of the geochemical model since they range between $10^{-2.5}$ and $10^{-2.1}$ bar. An alternative

experimental procedure for extracting pore waters and their dissolved gases has been used since 2000 in order to determine the content, origins and control processes of dissolved gases in pore water (Lassin et al., 2000, 2003; Gaucher et al., 2002, 2010; Girard et al., 2002, 2005; Huiban et al., 2009; Prinzhofer et al., 2009). The extraction procedure is based on outgassing claystone core samples in inert He or Ar gas, combined with analysis of the stable carbon isotopes. Numerous experiments performed on COx core samples confirm that the pCO_2 values range between $10^{-3.0}$ and $10^{-2.0}$ bar, and that the outgassed CO_2 is at equilibrium with the pore water, dissolved carbonate species and diagenetic carbonate minerals of the clay formation (Girard et al., 2005; Gaucher et al., 2010). However, from an experimental viewpoint, this method, like *in situ* monitoring and other techniques for extracting pore water from claystone, is not simple. The observed discrepancies are largely due to a lack of understanding the influence of physical sample properties on outgassing processes. As regards the pore water, this concerns its content and its state as free, capillary or bound water, whilst as regards the rock structure, it is about accessibility to its porosity and pore-size distribution. Such knowledge is of great interest not only for the outgassing experiment itself, but also for a better understanding of fluid diffusion and gas/water/rock interactions at the different interfaces between radioactive waste repository materials and the host claystone. The excavation when building a repository causes physical damage (the excavation damage zone, or EDZ), desaturation and partial oxidation of the surrounding claystone. Such damage affects both the rock structure and its hydro-mechanical behaviour (Matray et al., 2007; Charlier et al., 2013), as well as its transport properties by diffusion (Savoye et al., 2010).

Moreover, the concrete used for building access structures, drifts and containment materials for low- to intermediate radioactive waste undergoes carbonation processes when in contact with claystone. This is due mainly to the reaction of portlandite in the

cement with CO_2 via the carbonate system (Thiery et al., 2007; Trotignon et al., 2009) and to the huge contrast in pCO_2 between the cementitious materials and the claystone (Gaucher and Blanc, 2006; Gaboreau et al., 2012). Such mechanisms will also modify the diffusion and radionuclide-retention properties inside the concrete materials. All these considerations illustrate the need to correctly understand the role of CO_2 in the various conditions related to nuclear waste disposal issues.

2.2. GEOCHEMICAL MODEL FOR THE COx CLAYSTONE

The geochemical description of the equilibrium state of the COx minerals/water system uses the alternative model #1 of Gaucher et al. (2009), which relies on a mineralogical and cation exchange control of the pore-solution composition (Table 1). However, as the CO_2 outgassing/dissolution experiments carried out in the present study with various water contents are perturbations of the COx as compared to its reference state, we added the protonation/deprotonation surface complexation model of Bradbury and Baeyens (2009a, b) in order to take account of the pH buffering capacity of the lateral surfaces of clay minerals.

The amount of pore water remaining in the rock samples at various RH values was deduced from the hydration isotherm given later in Section 4.1. The evaporation process is implemented in the modelling so as to consider its impact on the chemical composition of the pore solution. In particular, the increasing ionic strength with decreasing water content is taken into account (e.g. increase of the Cl concentration).

Given the duration of the experiments, we only allowed assumed reactive minerals to (re-)precipitate; namely calcite, celestite and chalcedony. Other minerals initially present (illite, chlorite, quartz and pyrite) were only allowed to dissolve if the pore solution was under-saturated as far as they are concerned.

2.3. THERMODYNAMICS OF CHEMICAL REACTIVITY IN CAPILLARY SYSTEMS

The chemical behaviour of capillary systems has been studied for almost 20 years (Mercury and Tardy, 1997a, b; Zilberbrand, 1999) and the theoretical framework is now well established for calculating the standard thermodynamic properties of chemical compounds submitted to capillary pressure (Mercury and Tardy, 2001; Mercury et al., 2003; Lassin et al., 2005, 2014). In particular, capillary constraints are imposed on the system according to the Lassin et al. (2005) relationship for describing the equilibrium between vapour and capillary aqueous solution, namely:

$$RTln\frac{RH}{100} = RTln\frac{p_{vap}}{p_0} = RTlna_w + \int_{P_r}^{P} V_w \cdot dP' \qquad (1)$$

where R is the ideal gas constant (8.314472 J.mol^{-1}.K^{-1}), T is the absolute temperature (K), p_{vap} is the partial pressure of water vapour (Pa), p_0 is the saturation vapour pressure of water (Pa), a_w is the water activity (unitless), P is the internal pressure of liquid water (Pa), P_r is the reference pressure (10^5 Pa) and V_w is the molar volume of liquid water (m^3/mol).

Eq. 1 expresses the equality between the chemical potential of vapour (left-hand side) and that of a pore solution (right-hand side). It means that, in an unsaturated porous medium, various aqueous solutions can be at equilibrium with an atmosphere at a given RH. The two end members are *1)* a bulk solution at the reference pressure (P_r), with a chemical composition corresponding to a water activity a_w = RH/100, and *2)* pure water (a_w = 1) at an internal pressure P so that: $RTln\frac{RH}{100} = \int_{P_r}^{P} V_w \cdot dP'$. Any configuration in between can be envisaged, allowing the description of capillary aqueous solutions at equilibrium with more-or-less dry air in a porous medium. These pore solutions are characterized by a water activity of between 0 and 1 and by an internal pressure $P < P_r$ that verify Eq. 1.

Aqueous species are assumed to undergo the same pressure as water, and so any modification of their behaviour compared to a free aqueous solution is due to capillary the effects. These capillary pressure effects can be taken into account by applying the HKF equations (Helgeson et al., 1981; Tanger and Helgeson, 1988) for calculating the standard partial molar thermodynamic properties of aqueous species, as done by Mercury et al. (2003) and Lassin et al. (2005, 2014). The pressure dependence of the Gibbs energy $\Delta G_r(T,P)$ of an aqueous complexation reaction can thus be written as follows, considering for example the bicarbonate formation by combination of aqueous CO_2^0 with water:

$$CO_2^0 + H_2O \rightleftharpoons HCO_3^- + H^+ \quad (2)$$

$$\Delta G_r(T,P) = \Delta G_r^o(T,P_r) + RTln\left(\frac{a_{HCO_3^-}a_{H^+}}{a_{CO_2^0}a_{H_2O}}\right) + \int_{P_r}^{P} \Delta V_r^o(T,P') \cdot dP' \quad (3)$$

where $\Delta V_r^o(T,P') = V_{HCO_3^-}^o(T,P') + V_{H^+}^o(T,P') - V_{CO_2^0}^o(T,P') - V_{H_2O}^o(T,P')$. (4)

Eq. 4 represents the standard molar volume of reaction (2) at temperature T and pressure P', calculated from the standard partial molar volumes of the aqueous species involved in the reaction. In Eq. 3, $\Delta G_r^o(T,P_r)$ is the standard Gibbs energy of reaction at temperature T and the reference pressure P_r. The pressure effect on the activity coefficients of aqueous species is taken into account by the means of the pressure dependence of the Debye-Hückel coefficients (Lassin et al., 2005).

In addition, capillary systems offer specific features called anisobar contexts, where phases can undergo different pressures. This particularly applies to gas-solution equilibria since a gaseous compound cannot undergo negative pressures, whereas its aqueous equivalent is affected by the internal capillary water pressure, as is illustrated as follows by the dissolution reaction of gaseous CO_2(g):

$$CO_2(g) \rightleftharpoons CO_2^0 \quad (5)$$

The pressure dependence of reaction (5) is:

$$\Delta G_r(T,P) = \Delta G_r^o(T,P_r) + RTln\left(\frac{a_{CO_2^0}}{a_{CO_2(g)}}\right) + \int_{P_r}^{P} V_{CO_2^0}^o(T,P') \cdot dP' \quad (6)$$

where $a_{CO_2(g)} = {f_{CO_2(g)}}/{P_r} \approx {p}/{P_r}$ is the activity of CO_2(g), with $f_{CO_2(g)}$ being its fugacity and p its partial pressure, and where P is the internal pressure of capillary water. Fugacity and partial pressure are assumed equal when the gases behave ideally, as in our case.

A similar situation can be envisioned for minerals initially present in the rock matrix. They are submitted to the local pressure constraint when the porosity is saturated with water. The same pressure applies to these minerals during desaturation, regardless of the water content and thus of the capillary pressure. However, if the capillary aqueous solution is supersaturated with respect to a mineral, the latter should precipitate at the capillary water pressure. This can be illustrated by the dissolution/precipitation reaction of calcite ($CaCO_3$) in water:

$$CaCO_3 + H^+ \rightleftharpoons Ca^{2+} + HCO_3^- \quad (7)$$

The Gibbs energy of this reaction is:

$$\Delta G_r(T,P) = \Delta G_r^o(T,P_r) + RTln\left(\frac{a_{HCO_3^-}a_{Ca^{2+}}}{a_{H^+}}\right) + \int_{P_r}^{P} \Delta V_{r,aq}^o(T,P') \cdot dP' - \int_{P_r}^{P_{min}} V_{Calcite}^o(T,P') \cdot dP' \quad (8)$$

Where $\Delta V_{r,aq}^o(T,P') = V_{HCO_3^-}^o(T,P') + V_{Ca^{2+}}^o(T,P') - V_{H^+}^o(T,P')$, and P_{min} stands for the pressure exerted on the mineral. In the isobar case $P_{min} = P$, whereas in the anisobar case $P_{min} \neq P$. If $P_{min} = P_r$, then the volumetric contribution of the mineral phase vanishes

from Eq. 8 and only aqueous species contribute to the pressure dependence of the Gibbs energy of reaction (7).

The concept of an anisobaric context in capillary systems was first introduced by Mercury and Tardy (1997a) for describing the different shapes of ice crystals in fog droplets and in capillaries. Lassin et al. (2005) extended its application to water-unsaturated soils. Some evidence of the isobar/anisobar context in a capillary system was later obtained experimentally by Bouzid et al. (2011a). Note that this concept is also applied in other geoscience topics with their related specificities where water is under hydrostatic pressure while minerals are submitted to lithostatic pressure. For instance, one can evoke either theoretical and/or experimental studies about the smectite-to-illite transformation during diagenesis (Colten-Bradley, 1987), the formation of stylolites (Passchier and Trouw, 1996), the solution pressure effect (Renard and Ortoleva, 1997; Koehn et al., 2004, 2006; Anzalone et al., 2006) and the crystallization pressure effect (La Iglesia et al., 1997; Lopez-Acevedo et al., 1997; Scherer, 1999, 2004; Steiger, 2005a, b; Coussy, 2006; Osselin et al., 2013, 2014).

Because of the specific behaviour of aqueous species in a capillary context, the equilibrium conditions of every chemical reaction that involves such compounds may vary with capillary pressure. In particular, these should impact cation exchange reactions. Let us consider the Na^+-K^+ exchange reaction on exchanger X, representing a clay mineral:

$$X\text{-}Na + K^+ \rightleftharpoons X\text{-}K + Na^+ \quad (9)$$

The Gibbs energy of this reaction is:

$$\Delta G_r(T,P) = \Delta G_r^o(T,P_r) + RTln\left(\frac{a_{X-K}a_{Na^+}}{a_{X-Na}a_{K^+}}\right) + \int_{P_r}^{P} \Delta V_{r,aq}^o(T,P') \cdot dP' - \int_{P_r}^{P_{exch}} \Delta V_{r,exch}^o(T,P') \cdot dP' \quad (10)$$

where $\Delta V^o_{r,aq}(T,P') = V^o_{Na^+}(T,P') - V^o_{K^+}(T,P')$, $\Delta V^o_{r,exch}(T,P') = V^o_{X-K}(T,P') - V^o_{X-Na}(T,P')$ and P_{exch} stands for the pressure exerted on the cation exchanger. Here again, both the isobar and anisobar situations can be considered numerically. It is not clear, however, whether the isobar situation can be assumed since the interlayer cations in the clay minerals may not be subject to the capillary pressure as the aqueous species. On the other hand, the anisobar context occurs when $P_{exch} \neq P$. So if $P_{exch} = P_r$, the volumetric contribution of the cationic exchanger vanishes from Eq. 10. Then, only aqueous species contribute to the pressure dependence of the Gibbs energy and, thus, of the selectivity coefficient of reaction (9).

2.4. THERMODYNAMIC DATABASE

The well-known PhreeqC-2 geochemical calculation code (Parkhurst and Appelo, 1999) was used for calculating pCO_2 at equilibrium with the COx mineralogy and the pore water. Use of this code at temperatures and pressures different from the liquid-vapour saturation curve is possible if suitable and consistent thermodynamic databases are available. These were generated using the Thermo-ZNS code (Lassin et al., 2005) and include both isobar and anisobar mineral dissolution/precipitation reactions. The reference thermodynamic database implemented in Thermo-ZNS is the THERMODDEM database (Blanc et al., 2012) that provides information on critically selected standard thermodynamic properties of chemical compounds and reactions necessary for their calculation at various temperatures and pressures.

3. Materials and methods

3.1. MATERIALS

3.1.1. Description

Sample EST10273, representative of the claystone in the COx argillite, was selected for all the experiments made in this study. The sample was taken from borehole EST312 drilled in the Underground Research Laboratory (URL) of Bure, in the northeastern Paris Basin. The sampling depth was -177.49 m (Z_{NGF}; NGF: Nivellement Général de la France [*French Ordnance Datum Newlyn*]), corresponding to Unit C2b1 of Level C2b, which is the unit richest in clay minerals and the most homogeneous level in terms of porosity (Yven et al., 2007). The sample was packed in aluminium-foil vacuum bags in the field to prevent oxidation. The mineralogy and main physical properties of the sample are summarized in Table 2

The detailed mineralogy of the COx argillite from the URL has been described and discussed by Gaucher et al. (2004), Claret et al. (2004) and Clauer et al. (2007). The formation having undergone only limited burial (600 m) and diagenetic (T<50 °C) processes (Pellenard et al., 1999; ANDRA, 2005), the carbonate fraction is composed predominantly of calcite with minor dolomite, ankerite and siderite (Lerouge et al., 2011). It has a low organic matter content (<0.6%; Claret et al., 2005) that is immature in the petroleum sense (Elie et al., 2000). The COx mineral phases considered for the modelling were selected according to the model proposed by Gaucher et al. (2009).

The claystone of the COx argillite is characterized by a significant porosity (about 14% vol.) with a pore-size distribution ranging mostly between <1 nm and 0.2 µm (ANDRA, 2005; see also Leroy et al., 2007); it can, therefore, contain liquid water even under relatively dry conditions (see later).

3.1.2. Sample preparation

For the three series of experiments carried out in this study, Sample EST10273 was coarsely crushed and homogenized before separating out the 5 to 8 mm size fraction. The aim of this procedure was to maximize the surface area of the mineral assemblage in contact with the gas phase, without drastically changing the pore characteristics of the claystone. In other words, the objective was to favour mass transfer while preserving the specific 'water-content vs. suction' relationship of the rock. The sample was then maintained at ~100% RH in a hermetically closed container for a period of three months. No special caution was taken to prevent oxidation of the claystone during the saturation procedure; the desiccator was filled using ambient air. The study would thus be representative of processes occurring in desaturated EDZ around the ventilated galleries.

3.2. MEASUREMENT OF CO_2 PARTIAL PRESSURE AS A FUNCTION OF RH

Three sets of experiments were conducted on the EST10273 claystone sample in this study, with the experimental device shown on figure 1 being set up to measure the evolution of CO_2 partial pressure as a function of RH. The experiments were conducted at ambient temperature in cells filled with 100-200 g of fully saturated claystone sample (table 3). Wet argon (i.e. ~100% RH) was initially used to purge and fill the experimental device, following which the cells were flushed with a mixture of dry argon and water vapour to give initial RH values of 51, 68, 77, 85, 95 and 100%. The total pressure (>1 bar to avoid any pollution from outside the cell), temperature, CO_2 partial pressure and RH of each system were monitored throughout the experiments. The temperature remained almost constant, but was monitored for each sample (T~25 °C). The pCO_2 was measured by gas chromatography (CPG type Varian 3400), with pCO_2 measurement errors corresponding to 2σ, where σ is the standard deviation of the pCO_2 measured when equilibrium was assumed to be reached. Partial pressures of H_2S and

CH_4 were measured periodically for the absence of bacterial activity. The relative humidity was controlled by a HYGRASGARD® ESFF hygrometer probe associated with a JUMO di 08® type 701 531 digital display. The experimental errors in measuring the relative humidity were less than 3% when RH ranged between 40% and 60%, but rose to 5% when the RH value was outside this range. Thermodynamic equilibrium was assumed to be reached when both the partial pressure of CO_2 and RH remained stable over time. It should be noted that the gas volume of the bomb should be as small as possible for reducing the time required to reach equilibrium.

An initial condition of the experiments was the absence of gaseous CO_2 in the reactor. Therefore, the driving force affecting the system should be the degassing of CO_2, which in turn should affect the pore-water/minerals equilibrium. The different experimental conditions considered in this study are summarized in table 3. Experiment 1 ("Exp. 1") represents a series of wetting-drying cycles carried out on the same aliquot of the claystone sample, while Experiments 2 and 3 were carried out on different aliquots of the sample. In addition, two different-size reactors were used.

3.3. MEASUREMENT OF WATER CONTENT AS A FUNCTION OF RH

With the experimental setup shown in figure 1, and particularly where "Exp. 1" with several wetting-drying cycles is concerned (Table 3), it was not possible to simultaneously measure the water content of the COx samples and the pCO_2. We therefore carried out a preliminary calibration of the water content of the COx samples as a function of RH. Two samples, termed "Exp A" and "Exp B", were submitted to drying-wetting paths (Figure 2) with, for each measurement series, the starting point being fixed at an initial RH close to 100%, after which the RH was fixed at different values between 50% and 100%. The two samples were initially submitted to dehydration by flushing with dry argon, but this technique turned out to be ineffective

because of important gas consumption. The samples were therefore freeze-dried, with a wetting cycle then imposed on “Exp B” using salt solutions as proposed by Delage et al. (1998). Note that, as demonstrated by Delage and Pellerin (1984), the lyophilisation procedure (using a lyophiliser Christ Beta 2-8) has no significant impact on clay structures, but it does enable accurate measurements to be acquired of dry masses of COx material.

The water content c_w as a function of RH is calculated as follows:

$$c_w = \frac{m_w - m_{dry}}{100 \times m_{dry}} \quad (11)$$

where c_w is given in $g_{water}/100\ g_{claystone}$, m_w (in g) is the mass of the sample at a given RH, and m_{dry} (in g) refers to the mass of dry sample obtained by lyophilisation. The experimental conditions, as well as the salts used, are given in table 4.

It should be noted that the water transfer is carried out by steam water until equilibrium is reached, and therefore our calculations were made after stabilization of the sample mass. Moreover, we systematically measured all the RH values considered for calculation, only consulting the expected values given by Delage et al. (1998) for salt solutions in order to check the validity of our RH measurements.

4. Results

4.1. WATER CONTENT AS A FUNCTION OF RELATIVE HUMIDITY

The water content of the COx samples as a function of RH (i.e. the water retention curve) is shown on figure 3, along with data from Gaucher et al. (2006), Boulin (2008), Boulin et al. (2008) and Wan et al. (2013) for comparison. The literature data were selected because they were acquired on samples with a preserved pore structure, as we expect to be the case with our samples. A reasonable match is observed between the various experimental data, despite slight discrepancies; this is further discussed below.

4.2. PCO_2 EVOLUTION AS A FUNCTION OF TIME AND RH

With each experiment, the pCO_2 increased progressively with time in the gas phase, starting from nil CO_2 content until it reached a plateau. Figure 4 shows that this occurred after 458 days of "water/rock/gas" interactions for the 100% RH experiment (Exp. 2, Table 3) with the pCO_2 - COx claystone equilibrium being reached at 8.0 mbar, which agrees with the theoretical value of 10 mbar given by the model of Gaucher et al. (2009). All the experimental data obtained at various RHs are given in the electronic annex EA-1.

The time necessary to reach thermodynamic equilibrium depends on several parameters, such as the gas/solid ratio, the history of drying-rewetting cycles, etc. In this study it ranged between 4 months and 2 years (Table 5).

The equilibrium partial pressures of CO_2 obtained at different relative humidity values are given in Table 5, and the measured equilibrium pCO_2 plotted as a function of relative humidity is shown on figure *5* (diamonds). It can be seen that decreasing RH

significantly decreases pCO_2 at equilibrium with the claystone, the pCO_2 values measured at 50 and 100% RH varying by a factor of 10.

4.3. GEOCHEMICAL MODELLING

In order to interpret the experimental results and identify the mechanisms that control the observed changes in pCO_2, we applied the modelling procedure described in Section 2 to the following four scenarios.

Scenario 1: The only process assumed to be responsible for the change in equilibrium partial pressure of CO_2 is the increase in salinity resulting from evaporation of the pore water. The amount of evaporated water for each RH value is calculated from the water retention curve indicated in Section 4.1.

Scenario 2: In addition to evaporation and the increasing salinity, capillary constraints are imposed on the system in the simplest hypothesis of an isobaric context.

Scenario 3: An extension of Scenario 2, Scenario 3 aims at exploring the possibility that the selectivity constants of cation-exchange reactions depend on capillary pressure.

Scenario 4: This scenario considers that both anisobaric and isobaric cases can occur in the capillary porous system.

The calculated pCO_2 resulting from the geochemical modelling according to these four scenarios are given in table 5 and plotted on figure *5* for comparison with the experimental results. A first look at the data indicates that scenarios 2, 3 and 4 better reproduce the experimental data than Scenario 1, especially at low RH values; this is further discussed in Section 5.2.

Other model outputs, like pH and aqueous concentrations of dissolved elements (e.g. Ca, C, Na, K, Mg, Fe, Sr, Si, Al, S), provide further information about the chemical

behaviour of the COx-water-gas system. Unfortunately, these cannot be compared against experimental data since, to our knowledge, there is no reliable experimental method able to characterize the composition of various pore-water contents in the system studied here. For the interested reader, these model outputs are discussed in Electronic Annex EA-3 for each scenario.

5. Discussion

5.1. WATER CONTENT ISSUES

Wan et al. (2013), on measuring the water content of several COx samples (EST 43132, EST 43144, EST 43125, EST 43142), indicated that the samples were not fully hydrated due to water having evaporated during coring, storage and preparation. The degree of saturation (i.e. the ratio of water volume over pore volume) was 92-95%, with the water content being 7.3-7.6 g_{water}/100 $g_{claystone}$. Consequently, the amount of absorbed water in fully saturated samples can be estimated to be 7.9-8.0 g_{water}/100 $g_{claystone}$. This range of values agrees with data from Gaucher et al. (2006) and Boulin et al. (2008) (i.e. 8.04 and 7.56 g_{water}/100 $g_{claystone}$, respectively). However, Wan et al. (2013) also measured water contents ranging from 10.8 to 12.1 g_{water}/100 $g_{claystone}$ after three months of equilibration at almost 100% RH, and we obtained similar values (9.38 g_{water}/100 $g_{claystone}$) at 100% RH after three months of equilibration. Wan et al. (2013) thus concluded that the water content changes with the degree of saturation according to a bilinear function:

- The degree of saturation (s_w) increases linearly from 0 to 100% when the water content (c_w) increases from 0 to ~8 g_{water}/100 $g_{claystone}$, according to the relation $s_w = 12.5\ c_w$;
- Once the sample is fully saturated (s_w = 100), the water content can further increase up to 12.1 g_{water}/100 $g_{claystone}$.

Wan et al. (2013) also measured the evolution of porosity as a function of the degree of saturation. They demonstrated that a water content over 8 g_{water}/100 $g_{claystone}$ causes an increase in sample volume.

The small discrepancies between our present study and data from Boulin (2008) reflect a hysteresis effect (figure 3); Boulin (2008) measured water contents from drying paths, whereas our data measured at RH below ~90% were obtained from rewetting paths (Figure 2). It can thus be concluded that our data are consistent with the literature data, despite the fact that they were acquired on different samples. However, for reasons of consistency regarding the preparation methods used for all the experiments in this paper, only our data have been used to fit water content as a function of RH. For this we used the following expression (modified from Lassin, 2000):

$$c_w = \frac{a\left(p/p_0\right)+b\left(p/p_0\right)^2}{1+c\left(p/p_0\right)} + \frac{d\left(p/p_0\right)^2}{1-e\left(p/p_0\right)} \quad (12)$$

where p/p_0 is the relative partial pressure of water vapour (i.e. RH/100). This equation is an extension of the Langmuir isotherm, included in the first term of the right-hand side. It aims at empirically describing the following two points: *i*) multilayer adsorption and/or evolution of the interlayer water content (the quadratic part of the first term in the right-hand side of Eq. 12), and *ii*) the capillary water uptake at RH values above 30% (last term of the right-hand side of Eq. 12). The coefficients *a*, *b*, *c*, *d* and *e* are fitting parameters. Best-fit values (R^2=0.988 considering data measured during this study and that of Gaucher et al., 2006) are reported in Table 6.

Thanks to Eq. 12, the amount of water evaporated from the claystone sample to reach equilibrium with a given RH can be calculated for any RH value. It allows calculating the global salinity change in the pore solution, compared with the initial fully saturated state. The method does not discriminate the different compartments of water that exist within the porosity, namely pure capillary/mesoporal water, adsorbed/film water, interlayer water, and more-or-less strongly bound water (ANDRA, 2005). The distribution of these compartments is related to the geometry of the porosity with, during evaporation, the picture being further complicated by the fact that, as capillary water evaporates, its ionic

strength increases. As a result, the Debye length decreases and the capillary water/diffuse-layer volume ratio varies in a way that is difficult to characterize. Similarly, the interlayer water content of the clay minerals should decrease because of osmotic forces. But, to our knowledge, no existing methodology enables these different types of water to be discriminated in the COx rock as a function of water saturation and thus being able to rigorously take the evolution of the pore water chemistry into account.

5.2. pCO_2 EVOLUTION AS A FUNCTION OF RH

In this section the calculated partial pressures of pCO_2 resulting from the geochemical modelling are compared to the experimental results in order to identify the mechanisms that control the observed changes of pCO_2 as a function of RH. To this end, we successively discuss the four scenarios described in Section 4.3.

Scenario 1: Here, the model of Gaucher et al. (2009), augmented with the protonation/deprotonation reactions of Bradbury and Baeyens (2009a, b), is applied with a liquid/solid ratio representative of the water content at 100% RH given in Figure 3, i.e. 8 g_{water}/100 $g_{claystone}$. Then, using PhreeqC-2 (Parkhurst and Appelo, 1999), water is numerically extracted from the system down to a value corresponding to each target RH, as given by Eq. 12. The resulting equilibrium partial pressure of CO_2 is plotted on figure *5* (dashed line). The decreasing tendency of pCO_2 with decreasing RH is clear, but the discrepancy between calculated and measured values increases at low RH values. This indicates that an additional process may act on the system.

Note that the maximum mass loss, measured at 50% RH from the water content *vs*. RH diagram, is 6.7 g_{water}/100 $g_{claystone}$, which is close to 84% of the initial water. Concerning the impact on the pore water salinity, such a water loss increases the ionic strength of the pore solution from 0.086 to 0.359 eq/kgw. The corresponding water activity decreases from 0.998 to 0.992, which is inconsistent with the expected water activity of

0.5 at 50% RH. Here, again, there is an indication of a missing process in this first scenario that would compensate the gap between water activity and relative humidity.

These considerations represent but a first approximation since the different compartments of pore water (namely, capillary water, diffusion layers, interlayer water) should be distinguished (see discussion above). Nevertheless, if one assumes that evaporation mostly impacts capillary water so that the final ionic strength is about 1 eq/kgw (about 3 times the value obtained above), then the resulting water activity is around 0.97, which remains clearly inconsistent with the relative humidity of 50% imposed to the system.

Scenario 2: The left-hand side of Eq. 1 ($RTln\frac{RH}{100} = RTln\frac{p_{vap}}{p_0} = RTlna_w + \int_{P_r}^{P} V_w \cdot dP'$) gives the energetic contribution of a relative humidity of 50% as –1720 J.mol^{-1} of water at 25 °C. But the energetic contribution of a water activity of 0.992 is –20 J.mol^{-1} of water (first term of the right-hand side of Eq. 1). This means that, in the pore solution, the contribution of water activity due to the increase of salinity determined in Scenario 1 can be neglected as a first approximation. According to Eq. 1, the main energetic contribution in the pore solution should thus come from the pressure term $\int_{P_r}^{P} V_w \cdot dP'$. Neglecting the water activity term makes Eq. 1 into a form of the Kelvin law that is classically used for performing suction experiments (Delage et al., 1998).

Here, decreasing RH down to 50% provokes a decrease of the internal pore-water pressure to a value as low as –90 MPa. The resulting equilibrium pCO_2 calculated for the various target RH values are plotted on figure 5 (black full line). The contribution of the capillary constraints clearly improves the match between the model and the experimental data. It should also be noted that, as expected, there is no difference between the two scenarios at 100% RH.

Scenario 3: This scenario is an extension of Scenario 2. It aims at exploring the possibility that the selectivity coefficients of cation-exchange reactions depend on capillary pressure. To this end we took the anisobar situation (following the reasoning given in Section 2.3 about the use of Eq. 10) assuming that capillary constraints only affect the thermodynamic properties of the dissolved species (Na^+ and K^+ in the example, but also Ca^{2+}, Mg^{2+}, Fe^{2+} and Sr^{2+} in the simulation). The calculated pCO_2 at equilibrium with the COx mineralogical assemblage is plotted as a function of RH on figure *5* (grey full line). A slight, but insignificant, improvement compared to Scenario 2 is seen. Though the question of pressure dependence of the thermodynamic selectivity constants deserves being asked, our preliminary calculations do not enable us to conclude on their effective role with respect to pCO_2.

In addition to capillary pressure and ion activity coefficients in the pore solution, the increase in ionic strength due to evaporation of the water could further play a role in the cation exchange reactions. This has been shown by Liu et al. (2004) who considered the case of nitrate-type electrolyte solutions up to high concentrations. They proposed an approach for describing the change in the distribution of cations in the exchanger as a function of water activity. Unfortunately, their approach cannot be applied in the present case since it requires a specific parameter for every exchange reaction and every exchanger, and these parameters are not available for the system considered here. On the other hand, the water activity calculated in the pore solution corresponding to equilibrium with 50% RH is 0.992. This value is close to 1 and the cation-exchange reactions are not expected to be very sensitive to water activity in this range.

Scenario 4: In their experimental work and its theoretical interpretation, Bouzid et al. (2011a) showed that both anisobaric and isobaric contexts can occur in a capillary porous system, affecting its geochemical behaviour. They observed the formation of cubic crystals of halite in the cylindrical pores of polycarbonate filters initially filled with

NaCl brine and exposed to drying. When enough evaporation had occurred, a capillary situation took place: the brine was localised under cylindrically shaped capillary menisci in the spaces formed between the edges of the cubic crystal of halite and the pore wall. The edges of the salt then dissolved into the capillary solution in favour of a new solid that grew with the shape of the capillary meniscus. Because it was locally destabilized, Bouzid et al. (2011a) suggested that the cubic crystal of halite remained at the ambient pressure while in contact with capillary brine. On the other hand, the newly grown solid phase was assumed to be at the capillary pressure since it took the shape of the capillary meniscus.

Basically, the solubility of minerals under anisobaric conditions is generally greater than under isobaric conditions because of the volumetric difference between minerals and dissolved species. In the isobar configuration, the Gibbs energy of the mineral dissolution/precipitation reaction involves the volumetric contribution of all the chemical compounds of interest, including the solid phase (see Eq. 8). Because molar volumes of minerals are positive quantities, their volumetric contribution is energetically negative, and thus stabilizing, in capillary conditions (i.e. under negative pressures). On the other hand, in the anisobaric configuration, there is no volumetric contribution of the mineral to the Gibbs energy of the reaction (e.g. if the mineral is assumed at 10^5 Pa). Consequently, anisobaric minerals (i.e. minerals in their standard shape and crystallinity, with $P_{min} \neq P$) partly dissolve in favour of the isobar polymorphs (i.e. capillary solids with $P_{min} = P$) that are stabilized and can therefore precipitate. Anisobaric minerals can represent the initial mineralogy before capillary conditions have settled in the rock porosity, whereas isobaric minerals rather represent newly formed solids at mechanical equilibrium with the capillary pore water.

Because of these considerations, it appeared necessary to include the anisobar option in our study. This constitutes Scenario 4, since Scenario 2 is fully isobaric. In

Scenario 4, therefore, all minerals initially present in the COx model of Gaucher et al. (2009) are considered to be under anisobaric conditions, meaning that they are assumed to undergo a pressure of 10^5 Pa whatever the RH. Nevertheless, the assumed reactive minerals, such as calcite, celestite and chalcedony, are allowed to (re-)precipitate under isobaric conditions.

These hypotheses have led to results identical to those obtained for Scenario 2 for the following reasons:

- Numerically, all primary anisobaric calcite and celestite have been converted to their more stable isobaric polymorphs. The final control for calcite and celestite is thus exerted by the isobaric phases as in Scenario 2.
- As in Scenario 2, chalcedony precipitates and controls Si concentration at RH values below 95%. This is due to water evaporation and the consecutive increase of Si concentration, initially at equilibrium with quartz for RH=100%. Since chalcedony is a secondary phase, it is considered in the isobaric context in both scenarios 2 and 4.
- For pyrite, chlorite and illite, water evaporation supersaturates the pore solution with respect to these minerals since, by definition, it was at equilibrium at 100% RH. Whatever the isobaric or anisobaric context, evaporation stops the dissolution of these minerals, resulting in the same final concentrations in scenarios 2 and 4.

The calculated equilibrium pCO_2 values for Scenario 4 are also plotted in figure 5, but are merged with those obtained for Scenario 2.

We can thus summarize the modelling part of this work as follows: the calculations involve all the geochemical contributions evoked in Section 2.2, both without (see Scenario 1) and with (see Scenario 2) the effect of capillary pressure on the chemical

equilibria. Better results are clearly obtained when considering capillary pressure. The decrease of pCO_2 with RH (indicated by the dashed line in figure 5) is due to the increase in ionic strength in the pore solution resulting from water evaporation and is in accordance with a salting-out effect. It is not, however, sufficient to explain the experimental measurements. The simple introduction of capillary constraints shifts the curve (full line in Fig. 5) so that it closely fits the experimental data. As expected, there is no difference between the two calculations at saturation, and discrepancies increase as RH decreases. In both series of calculations, the pH is buffered between 7.13 and 7.15 as a result of the protonation/deprotonation surface reactions (see Electronic Annex EA-3 for further details). One of the main features is the isobar/anisobar behaviour of minerals. Anisobar minerals are destabilized by capillary pressure, and partly dissolve in favour of the isobar polymorphs that are stabilized and can therefore precipitate. Given the duration of the experiments, as well as the investigated temperature, only assumed reactive minerals were able to re-precipitate, namely calcite, celestite and chalcedony (if possible after anisobaric quartz had dissolved); other minerals initially present (illite, chlorite, and pyrite) were only allowed to dissolve. These mass transfers, combined with aqueous speciation and CO_2 solubility variations, all contribute in a consistent fashion to the calculated equilibrium pCO_2.

6. Concluding remarks

The experimental results obtained in this study were reproduced by calculation without any parameter adjustment. They highlight the significant impact of capillary pressure on chemical equilibria in partially water-saturated porous media. Our results further demonstrate that the theoretical principles of capillary geochemistry still hold in complex geochemical systems such as the COx claystone. This strongly supports and motivates their application to other natural and industrial systems where capillary phenomena may occur, namely in finely porous systems subject to drying. For instance, this may concern

acid mine drainage and the formation of passivating layers of gypsum on calcite grains, so that acid leachate can percolate down sulphidic waste rock dumps without being buffered (Pedretti et al., 2015). According to Mercury et al. (2004), the capillary pressure of water may also be a prominent parameter controlling the addition of atmospheric noble gases to ground water. As shown by these authors, considering capillary phenomena can help in reconstructing paleotemperatures from datasets of noble gas contents in ground water. In the context of global climate change, the behaviour of gases trapped in the warming permafrost is an issue (Koven et al., 2011), and here the consideration of capillary phenomena could help in estimating gas budgets, in particular those related to the greenhouse effect. According to the study of Henry et al. (1999), the stability of clathrates, such as methane hydrate, is partly controlled by capillary phenomena that can take place in marine sediments. This suggests that other types of clathrate, like carbon dioxide hydrate, could also be concerned. In the context of oil and gas reservoirs, the increasing pressure of hydrocarbon with time may dry the caprock and consequently modify its chemistry because of induced capillary phenomena. As another example, one can evoke issues concerning the succession of drying-wetting events on the durability of rocks and building materials (Gökceoğlu et al., 2000), which may involve the alternation of capillary phenomena and crystallization, or swelling pressure constraints, in the porosity (Osselin et al., 2014).

The present study also illustrates the utility of geochemical modelling in complex systems for which experimental data are challenging to acquire. For example, the low water content in unsaturated porous media makes it difficult to take representative, and thus meaningful, water samples. Moreover, the potentially limited mass transfers, due to the limited amounts of water held in such systems, make the geochemical and mineralogical evolutions observable only over very long timeframes.

The robustness of our approach in the particular system of the COx claystone will be further evaluated through new experiments. Firstly, an additional type of initial condition will be imposed in the reactor, with an initial overpressure of CO_2 (compared to the expected equilibrium pCO_2). We expect achievement of the thermodynamic equilibrium in this experiment to be driven by CO_2 dissolution in the pore water and a consecutive interaction with the mineralogical assemblage. The final expected value of pCO_2 is the same as in the experiment carried out with the same RH, but starting from zero CO_2 content in the gas phase. Such a result would provide strong evidence that thermodynamic equilibrium is achieved. This proposed experiment should also provide interesting results regarding the alteration of clayey cap rock by CO_2 in the context of geological carbon sequestration (e.g. Bourg et al., 2015).

Secondly, the same experiments will be carried out at higher temperatures. Here we expect that this will accelerate chemical reactions, allowing the acquisition of more data points, while also allowing the model to be validated at different temperatures. In addition, a large experimental dataset should provide useful information that can be used for investigating the reaction kinetics.

Acknowledgements

This study was supported financially by the French National Radioactive Waste Management Agency (ANDRA) and the French Geological Survey (BRGM). We warmly thank Ian C. Bourg and two anonymous reviewers who greatly helped improve the scientific quality of the paper.

We are very grateful to Dr. H.M. Kluijver and Dr. P. Skipwith who improved the English of this article.

References

Altmann S., Tournassat C., Goutelard F., Parneix J. C., Gimmi T. and Maes N. (2012) Diffusion-driven transport in clayrock formations. *Applied Geochemistry* **27**, 463-478.

ANDRA (2005) *Dossier 2005 Argile. Synthesis: Evaluation of the feasibility of a geological repository in an argillaceous formation. Meuse/Haute-Marne site*. ISBN 2-916162-00-3, ANDRA, Châtenay-Malabry, France, 2005, 239 p.

Anzalone A., Boles J., Greene G., Young K., Israelachvili J. and Alcantar N. (2006) Confined fluids and their role in pressure solution. *Chemical Geology* **230**, 220-231.

Berkeley P. and Carey V. P. (2013) Thermodynamic analysis of wall effects on phase stability and homogeneous nucleation in nanochannels containing superheated liquid. *Nanoscale and Microscale Thermophysical Engineering* **17**, 281-303.

Blanc P., Lassin, A., Piantone P., Azaroual M., Jacquemet N., Fabbri A. and Gaucher E. C. (2012) Thermoddem: A geochemical database focused on low temperature water/rock interactions and waste materials. *Applied Geochemistry* **27**, 2107-2116.

Boulin P. F. (2008) *Expérimentation et Modélisation du Transfert d'hydrogène à travers des argiles de centre de stockage de déchets radioactifs*. Ph.D. Thesis, Institut Polytechnique de Grenoble, Laboratoire d'études des Transferts en Hydrologie et Environnement, France, 316 p.

Boulin P. F., Angulo-Jaramillo R., Daian J. F., Talandier J. and Berne P. (2008) Experiments to estimate gas intrusion in Callovo-oxfordian argillites. *Physics and Chemistry of the Earth, Parts A/B/C* **33**, S225-S230.

Bourg I. C., Beckingham L. E. and DePaolo D. J. (2015) The nanoscale basis of CO_2 trapping for geologic storage. *Environmental Science & Technology* **49**, 10265-10284.

Bouzid M., Mercury L., Lassin A., Matray J. M. and Azaroual M. (2011a) In-pore tensile stress by drying-induced capillary bridges inside porous materials. *Journal of Colloid and Interface Science* **355**, 494-502.

Bouzid M., Mercury L., Lassin A. and Matray J. M. (2011b) Salt precipitation and trapped liquid cavitation in micrometric capillary tubes. *Journal of Colloid and Interface Science* **360**, 768-776.

Bradbury M. H. and Baeyens B. (2009a) Experimental and modelling studies on the pH buffering of MX-80 bentonite porewater. *Applied Geochemistry* **24**, 419-425.

Bradbury M. H. and Baeyens B. (2009b) Sorption modelling on illite Part I: Titration measurements and the sorption of Ni, Co, Eu and Sn. *Geochimica et Cosmochimica Acta* **73**, 990-1003.

Charlier R., Collin F., Pardoen B., Talandier J., Radu J.-P. and Gerard P. (2013) An unsaturated hydro-mechanical modelling of two in-situ experiments in Callovo-Oxfordian argillite. *Engineering Geology* **165**, 46-63.

Claret F., Sakharov B. A., Drits V. A., Velde B., Meunier A., Griffault L. and Lanson B. (2004) Clay minerals in the Meuse - Haute Marne underground laboratory (France): Possible influence of organic matter on clay mineral evolution. *Clays and Clay Minerals* **52**, 515-532.

Claret F., Schäfer T., Rabung T., Wolf M., Bauer A. and Buckau G. (2005) Differences in properties and Cm (III) complexation behavior of isolated humic and fulvic acid derived from Opalinus clay and Callovo-Oxfordian argillite. *Applied Geochemistry* **20**, 1158-1168.

Clauer N., Fourcade S., Cathelineau M., Girard J. P., Vincent B., Elie M., Buschaert S. and Rousset D. (2007) A review of studies on the diagenetic evolution of the Dogger-to-Tithonian sedimentary sequence in the eastern Paris Basin - impact on the physical and chemical rock properties. *Mém. Soc. Géol. France* **178**, 59-71.

Colten-Bradley V. A. (1987) Role of pressure in smectite dehydration: Effects on geopressure and smectite-to-illite transformation. *American Association of Petroleum Geologists Bulletin* **71**, 1414-1427.

Coudrain-Ribstein A. and Gouze P. (1993) Quantitative study of geochemical processes in the Dogger aquifer, Paris Basin, France. *Applied Geochemistry* **8**, 495-506.

Coudrain-Ribstein A., Gouze P. and de Marsily G. (1998) Temperature-carbon dioxide partial pressure trends in confined aquifers. *Chemical Geology* **145**, 73-89.

Coussy O. (2006) Deformation and stress from in-pore drying-induced crystallization of salt. *Journal of the Mechanics and Physics of Solids* **54**, 1517-1547.

Delage P. and Pellerin F. (1984) Influence de la lyophilisation sur la structure d'une argile sensible du Québec. *Clay Minerals* **19**, 151-160.

Delage P., Howat M.D. and Cui Y.J. (1998) The relationship between suction and swelling properties in a heavily compacted unsaturated clay. *Engineering Geology* **50**, 31-48.

Delay J., Rebours H., Vinsot A. and Robin P. (2007) Scientific investigation in deep wells for nuclear waste disposal studies at the Meuse/Haute Marne underground research laboratory, northeastern France. *Physics and Chemistry of the Earth, Parts A/B/C* **32**, 42-57.

Elie M., Faure P., Michels R., Landais P. and Griffault L. (2000) Natural and laboratory oxidation of low-organic-carbon-content sediments: comparison of chemical changes in hydrocarbons. *Energy & Fuels* **14**, 854-861.

Gaboreau S., Lerouge C., Dewonck S., Linard Y., Bourbon X., Fialips C. I., Mazurier A., Prêt D., Borschneck D., Montouillout V., Gaucher E. C. and Claret F. (2012) In-situ interaction of cement paste and shotcrete with claystones in a deep disposal context. *American Journal of Science* **312**, 314-356.

Gaucher E. C. and Blanc P. (2006) Cement/clay interactions - A review: Experiments, natural analogues, and modeling. *Waste Management* **26**, 776-788.

Gaucher E. C., Crouzet C., Flehoc C., Girard J.-P. and Lassin A. (2002) *Measurement of partial pressure and isotopic composition of CO_2 on two core samples from the Mont Terri Rock Laboratory, borehole BPC-1*. BRGM Report/RP-51771-FR, 26 p.

Gaucher E. C., Robelin C., Matray J.-M., Négrel G., Gros Y., Heitz J.-F., Vinsot A., Rebours H., Cassagnabère A. and Bouchet A. (2004) ANDRA underground research laboratory: interpretation of the mineralogical and geochemical data acquired in the Callovian-Oxfordian formation by investigative drilling. *Physics and Chemistry of the Earth* **29**, 55-77.

Gaucher E. C., Blanc P., Bardot F., Braibant G., Buschaert S., Crouzet C., Gautier A., Girard J.-P., Jacquot E., Lassin A., Negrel G., Tournassat C., Vinsot A. and Altmann S. (2006) Modelling the porewater chemistry of the Callovian–Oxfordian formation at a regional scale. *Comptes Rendus Geoscience* **338**, 917-930.

Gaucher E. C., Tournassat C., Pearson F. J., Blanc P., Crouzet C., Lerouge C. and Altmann S. (2009) A robust model for pore-water chemistry of clayrock. *Geochimica et Cosmochimica Acta* **73**, 6470-6487.

Gaucher E. C., Lassin A., Lerouge C., Fléhoc C., Marty N. C. M., Henry B., Tournassat C., Altmann S., Vinsot A., Buschaert S., Matray J. M., Leupin O. X. and de Craen M. (2010) CO_2 partial pressure in clayrocks: A general model. In. *Water-rock Interaction WRI-13*, Aug 2010, Guanajuato, Mexico (eds. P. Birkle and I. Torres-Alvarado). Taylor & Francis Group (CRC Press), 855-858.

Girard J.-P., Fléhoc C., Gaucher E., Prinzhofer A. and Chappellaz J. (2002) *Caractérisation isotopique des gaz émis par les argilites du Callovo-Oxfordien (projet Isogaz, phase 1)*. BRGM Report/ RP-51640-FR, 42 p.

Girard J.-P., Fléhoc C. and Gaucher E. (2005) Stable isotope composition of CO_2 outgassed from cores of argillites: a simple method to constrain δ18O of porewater and $\delta^{13}C$ of dissolved carbon in mudrocks. *Applied Geochemistry* **20**, 713-725.

Gökceoğlu C., Ulusay R. and Sönmez H. (2000) Factors affecting the durability of selected weak and clay-bearing rocks from Turkey, with particular emphasis on the influence of the number of drying and wetting cycles. *Engineering Geology* **57**, 215-237.

Helgeson H. C., Kirkham D. H. and Flowers G. C. (1981) Theoretical prediction of the thermodynamic behavior of aqueous electrolytes at high pressures and temperatures: IV. Calculation of activity coefficients, osmotic coefficients, and apparent molal and standard and relative partial molal properties to 600°C and 5 kb. *American Journal of Science* **281**, 1249-1516.

Henry P., Thomas M. and Clennell M. B. (1999) Formation of natural gas hydrates in marine sediments: 2. Thermodynamic calculations of stability conditions in porous sediments. *Journal of Geophysical Research: Solid Earth* **104**, 23005-23022.

Huiban Y., Noirez S., Prinzhofer A., Girard J. P. and Chappellaz J. (2009) Chemical and isotopic analysis of hydrocarbon gas at trace levels: Methodology and results. *Chemical Geology* **265**, 363-368.

Koehn D., Dysthe D. K. and Jamtveit B. (2004) Transient dissolution patterns on stressed crystal surfaces. *Geochimica et Cosmochimica Acta* **68**, 3317-3325.

Koehn D., Malthe-Sørenssen A. and Passchier C. W. (2006) The structure of reactive grain-boundaries under stress containing confined fluids. *Chemical Geology* **230**, 207-219.

Koven C. D., Ringeval B., Friedlingstein P., Ciais P., Cadule P., Khvorostyanov D., Krinner G. and Tarnocai C. (2011) Permafrost carbon-climate feedbacks accelerate global warming. *Proceedings of the National Academy of Sciences* **108**, 14769-14774.

La Iglesia A., Gonzalez V., Lopez-Acevedo V. and Viedma C. (1997) Salt crystallization in porous construction materials. I Estimation of crystallization pressure. *Journal of Crystal Growth* **177**, 111-118.

Landais P. (2006) Advances in geochemical research for the underground disposal of high-level, long-lived radioactive waste in a clay formation. *Journal of Geochemical Exploration* **88**, 32-36.

Lassin A. (2000) *Thermodynamique de l'hydratation et modélisation de la stabilité des argiles. Application à la pédogenèse climatique et à la diagenèse hydrothermale*. Ph.D. Thesis, Louis Pasteur University; Documents du BRGM n° **296**, p. 209.

Lassin A., Gaucher E. and Crouzet C. (2000) *Measurements of partial pressure of CO_2 and alcanes in core samples of Opalinus Clay from Benken, Switzerland*. BRGM Report/RC-50537-FR, 39 p.

Lassin A., Gaucher E. and Crouzet C. (2003) Dissolved carbon dioxide and hydrocarbon extraction. Annex 6. In: Pearson F. J. et al., *Geochemistry of water in the Opalinus Clay Formation at the Mont Terri Rock Laboratory. Geology Series 5, Swiss Federal Office for Water and Geology*, p. 319

Lassin A., Azaroual M. and Mercury L. (2005) Geochemistry of unsaturated soil systems: Aqueous speciation and solubility of minerals and gases in capillary solutions. *Geochimica et Cosmochimica Acta* **69**, 5187-5201.

Lassin A., Dymitrowska M. and Azaroual M. (2011) Hydrogen solubility in pore water of partially saturated argillites: Application to Callovo-Oxfordian clayrock in the context of a nuclear waste geological disposal. *Physics and Chemistry of the Earth, Parts A/B/C* **36**, 1721-1728.

Lassin A., Marty N. C. M., Henry B., Trémosa J., Gailhanou H., Madé B., Altmann S. and Gaucher E. C. (2013) Equilibrium Partial Pressure of CO_2 in the Callovo-Oxfordian Argillite as a Function of Relative Humidity. *Procedia Earth and Planetary Science* **7**, 459-462.

Lassin A., Mercury L. and Azaroual M. (2014) Geochemistry of capillary hydrogeochemical systems in arid environments. *In: Transport and Reactivity of Solutions in Confined Hydrosystems* (eds. L. Mercury, N. Tas and M. Zilberbrand). Springer Netherlands, pp. 213-221.

Lerouge C., Grangeon S., Gaucher E. C., Tournassat C., Agrinier P., Guerrot C., Widory D., Fléhoc C., Wille G., Ramboz C., Vinsot A. and Buschaert S. (2011) Mineralogical and isotopic record of biotic and abiotic diagenesis of the Callovian–Oxfordian clayey formation of Bure (France). *Geochimica et Cosmochimica Acta* **75**, 2633-2663.

Leroy P., Revil A., Altmann S. and Tournassat C. (2007) Modeling the composition of the pore water in a clay-rock geological formation (Callovo-Oxfordian, France). *Geochimica et Cosmochimica Acta* **71**, 1087-1097.

Letellier P. and Turmine M. (2013) Solubility of gas in confined systems. Nonextensive thermodynamics approach. *Journal of Colloid and Interface Science* **392**, 382-387.

Liu C., Zachara J.M. and Smith S.C. (2004) A cation exchange model to describe Cs^+ sorption at high ionic strength in subsurface sediments at Hanford site, USA. *Journal of Contaminant Hydrology* **68**, 217-238.

Lopez-Acevedo V., Viedma C., Gonzalez V. and La Iglesia A. (1997) Salt crystallization in porous construction materials. II. Mass transport and crystallization processes. *Journal of Crystal Growth* **182**, 103-110.

Marty N. C. M., Tournassat C., Burnol A., Giffaut E. and Gaucher E. C. (2009) Influence of reaction kinetics and mesh refinement on the numerical modelling of concrete/clay interactions. *Journal of Hydrology* **364**, 58-72.

Marty N. C. M., Bildstein O., Blanc P., Claret F., Cochepin B., Gaucher E. C., Jacques D., Lartigue J.-E., Liu S., Mayer K. U., Meeussen J. C. L., Munier I., Pointeau I., Su D. and Steefel C. I. (2015) Benchmarks for multicomponent reactive transport across a cement/clay interface. *Computers & Geosciences* **19**, 635-653.

Matray J. M., Savoye S. and Cabrera J. (2007) Desaturation and structure relationships around drifts excavated in the well-compacted Tournemire's argillite (Aveyron, France). *Engineering Geology* **90**, 1-16.

Mercury L. and Tardy Y. (1997a) Caractéristiques physicochimiques de l'eau capillaire et des gouttelettes de brouillard. *Compte-rendus de l'Académie des Sciences, Paris* **325**, 947-954.

Mercury L. and Tardy Y. (1997b) Pression négative et propriétés thermodynamiques de l'eau capillaire. "Le point sur…". *Compte-rendus de l'Académie des Sciences, Paris* **324** (IIa), 863-873.

Mercury L. and Tardy Y. (2001) Negative pressure of stretched liquid water. Geochemistry of soil capillaries. *Geochimica et Cosmochimica Acta* **65**, 3391-3408.

Mercury L., Azaroual M., Zeyen H. and Tardy Y. (2003) Thermodynamic properties of solutions in metastable systems under negative or positive pressures. *Geochimica et Cosmochimica Acta* **67**, 1769-1785.

Mercury L., Pinti D. L. and Zeyen H. (2004) The effect of the negative pressure of capillary water on atmospheric noble gas solubility in ground water and palaeotemperature reconstruction. *Earth & Planetary Science Letters* **223**, 147-161.

Miachon S., Syakaev V. V., Rakhmatullin A., Pera-Titus M., Caldarelli S. and Dalmon J.-A. (2008) Higher Gas Solubility in Nanoliquids? *ChemPhysChem* **9**, 78-82.

Osselin F., Fen-Chong T., Fabbri A., Lassin A., Pereira J.-M. and Dangla P. (2013) Dependence on injection temperature and on aquifer's petrophysical properties of the local stress applying on the pore wall of a crystallized pore in the context of CO_2 storage in deep saline aquifers. *The European Physical Journal - Applied Physics* **64**, 21101.

Osselin F., Fabbri A., Fen-Chong T., Dangla P., Pereira J.-M. and Lassin A. (2015) Stress from NaCl crystallisation by carbon dioxide injection in aquifers. *Environmental Geotechnics* **2** (5), 280-291. http://dx.doi.org/10.1680/envgeo.13.00057.

Parkhurst D. L. and Appelo C. A. J. (1999) *User's Guide to PHREEQC (version 2): A Computer Program for Speciation, Batch-reaction, One-dimensional Transport, and Inverse Geochemical Calculations*. U.S. Department of the Interior, U.S. Geological Survey.

Passchier C. W. and Trouw R. A. J. (1996) *Micro-tectonics*. Springer-Verlag, Berlin, Heidelberg, New-York, 289 p.

Pearson F., Tournassat C. and Gaucher E. C. (2011) Biogeochemical processes in a clay formation in situ experiment: Part E–Equilibrium controls on chemistry of pore water from the Opalinus Clay, Mont Terri Underground Research Laboratory, Switzerland. *Applied geochemistry* **26**, 990-1008.

Pedretti D., Lassin A. and Beckie R. D. (2015) Analysis of the potential impact of capillarity on long-term geochemical processes in sulphidic waste-rock dumps. *Applied Geochemistry* **62**, 75-83. http://dx.doi.org/10.1016/j.apgeochem.2015.03.017

Pellenard P., Deconinck J. F., Marchand D., Thierry J., Fortwengler D. and Vigneron G. (1999) Contrôle géodynamique de la sédimentation argileuse du Callovien-Oxfordien moyen dans l'Est du bassin de Paris: influence eustatique et volcanique. *Comptes Rendus de l'Académie des Sciences - Earth and Planetary Science* **328** (IIa), 807-813.

Prinzhofer A., Girard J. P., Buschaert S., Huiban Y. and Noirez S. (2009) Chemical and isotopic characterization of hydrocarbon gas traces in porewater of very low permeability rocks: The example of the Callovo-Oxfordian argillites of the eastern part of the Paris Basin. *Chemical Geology* **260**, 269-277.

Renard F. and Ortoleva P. (1997) Water films at grain-grain contacts: Debye-Hückel, osmotic model of stress, salinity, and mineralogy dependence. *Geochimica and Cosmochimica Acta* **61**, 1963-1970.

Savoye S., Page J., Puente C., Imbert C. and Coelho D. (2010) New Experimental Approach for Studying Diffusion through an Intact and Unsaturated Medium: A Case Study with Callovo-Oxfordian Argillite. *Environmental Science & Technology* **44**, 3698-3704.

Scherer G. W. (1999) Crystallisation in pores. *Cement and Concrete Research* **29**, 1347-1358.

Scherer G .W. (2004) Stress from crystallization of salt. *Cement and Concrete Research* **34**, 1613-1624.

Steiger M. (2005a) Crystal growth in porous materials - I: The crystallization pressure of large crystals. *Journal of Crystal Growth* **282**, 455-469.

Steiger M. (2005b) Crystal growth in porous materials - II: Influence of crystal size on the crystallization pressure. *Journal of Crystal Growth* **282**, 470-481.

Tanger J .C. IV and Helgeson H. C. (1988) Calculation of the thermodynamic and transport properties of aqueous species at high pressures and temperatures: Revised equations of state for the standard partial molal properties of ions and electrolytes. *American Journal of Science* **288**, 19-98.

Thiery M., Villain G., Dangla P. and Platret G. (2007) Investigation of the carbonation front shape on cementitious materials: Effects of the chemical kinetics. *Cement and Concrete Research* **37**, 1047-1058.

Thury M. and Bossart P. (1999) The Mont Terri rock laboratory, a new international research project in a Mesozoic shale formation, in Switzerland. *Engineering Geology* **52**, 347-359

Tournassat C., Lerouge C., Blanc P., Brendlé J., Greneche J.M., Touzelet S. and Gaucher E. C. (2008) Cation exchanged Fe(II) and Sr compared to other divalent cations (Ca, Mg) in the Bure Callovian–Oxfordian formation: Implications for porewater composition modelling. *Applied Geochemistry* **23**, 641-654.

Tournassat C., Vinsot A., Gaucher E. C. and Altmann S. (2015) Chapter 3 - Chemical Conditions in Clay-Rocks. In*: Developments in Clay Science* s. C. Tournassat, C. I. Steefel, I. C. Bourg and F. Bergaya). Elsevier, pp. 71-100.

Trotignon, L., Devallois V., Peycelon H., Tiffreau C. and Bourbon X. (2007) Predicting the long term durability of concrete engineered barriers in a geological repository for radioactive waste. *Physics and Chemistry of the Earth, Parts A/B/C* **32**, 259-274.

Trotignon L., Thouvenot P., Munier I., Cochepin B., Piaul, E., Treille E., Bourbon X. and Mimid S. (2009) *Numerical simulation of atmospheric carbonation of concrete components in a deep geological radwaste disposal site during operating period using Toughreact*. TOUGH Symposium, Berkeley, California, Lawrence Berkeley National Laboratory, 14-16 Sept. 2009.

Vieillard P., Ramırez S., Bouchet A., Cassagnabere A., Meunier A., and Jacquot E. (2004) Alteration of the Callovo-Oxfordian clay from Meuse-Haute Marne Underground Laboratory (France) by alkaline solution: II. Modelling of mineral reactions. *Applied Geochemistry* **19**, 1699-1709.

Vinsot A., Mettler S. and Wechner S. (2008) In situ characterization of the Callovo-Oxfordian pore water composition. *Physics and Chemistry of the Earth, Parts A/B/C* **33**, S75-S86.

Wan M., Delage P., Tang A. M. and Talandier J. (2013) Water retention properties of the Callovo-Oxfordian claystone. *International Journal of Rock Mechanics and Mining Sciences* **64**, 96-104.

Yven B., Sammartino S., Géraud Y., Homand F. and Villiéras F. (2007) Mineralogy, texture and porosity of Callovo-Oxfordian argillites of the Meuse/Haute-Marne region (eastern Paris Basin). *Mémoires de la Société géologique de France* **178**, 73-90.

Zilberbrand M. (1999) On Equilibrium Constants for Aqueous Geochemical Reactions in Water Unsaturated Soils and Sediments. *Aquatic Geochemistry* **5**, 195-206.

Tables

Figure captions

Figure 1: Schematic representation of the experimental setup.

Figure 2: Drying-wetting paths applied for the determination of water content in the COx samples as a function of RH.

Figure 3: Evolution of the water content of COx claystone (g_{water}/100 $g_{claystone}$) as a function of relative humidity (RH). Symbols represent experimental measurements; triangles are water-sorption test data acquired in this study on EST312 argillite samples (closed black triangle = sample 1; open triangles = sample 2); the open square is from Gaucher et al. (2006) on an EST312 argillite sample; closed black circles are sorption-test data acquired by Boulin et al. (2008) on EST25301 argillite samples; open circles are VARIMASS sorption-test data acquired by Boulin (2008) on EST25301 argillite samples; full grey diamonds are calculated from EST-43125-4144 samples (Wan et al., 2013); the full line represents the fit of the experimental results obtained for the EST312 samples.

Figure 4: Evolution with time of pCO_2, for the 100% RH experiment (Exp. 2). The grey dashed-line represents pCO_2 assumed at equilibrium with the COx.

Figure 5: Evolution of the partial pressure of CO_2 (pCO_2) as a function of the relative humidity (RH). Symbols are experimental data and lines are model calculations. See text for the different scenarios.

Electronic Annexes

Electronic Annex EA-1. pCO_2 monitoring during experiments at various RHs at room temperature

Electronic Annex EA-2. Thermodynamic database, in PhreeqC-2 format, used for geochemical calculations and PhreeqC input files

Electronic Annex EA-3. Evolution of solution properties (other than pCO_2) as a function of RH

Lassin et al. (2016) "Equilibrium partial pressure of CO_2 in Callovian-Oxfordian argillite as a function of relative humidity: experiments and modelling"

Figure captions

Figure 6: Schematic representation of the experimental setup.

Figure 7: Drying-wetting paths applied for the determination of water content in the COx samples as a function of RH.

Figure 8: Evolution of the water content of COx claystone (g_{water}/100 $g_{claystone}$) as a function of relative humidity (RH). Symbols represent experimental measurements; triangles are water-sorption test data acquired in this study on EST312 argillite samples (closed black triangle = sample 1; open triangles = sample 2); the open square is from Gaucher et al. (2006) on an EST312 argillite sample; closed black circles are sorption-test data acquired by Boulin et al. (2008) on EST25301 argillite samples; open circles are VARIMASS sorption-test data acquired by Boulin (2008) on EST25301 argillite samples; full grey diamonds are calculated from EST-43125-4144 samples (Wan et al., 2013); the full line represents the fit of the experimental results obtained for the EST312 samples.

Figure 9: Evolution of pCO_2 with time for the 100% RH experiment (Exp. 2). The grey dashed-line represents pCO_2 assumed at equilibrium with the COx.

Figure 10: Evolution of the partial pressure of CO_2 (pCO_2) as a function of the relative humidity (RH). Symbols are experimental data and lines are model calculations. See text for the different scenarios.

Figures

Figure 1

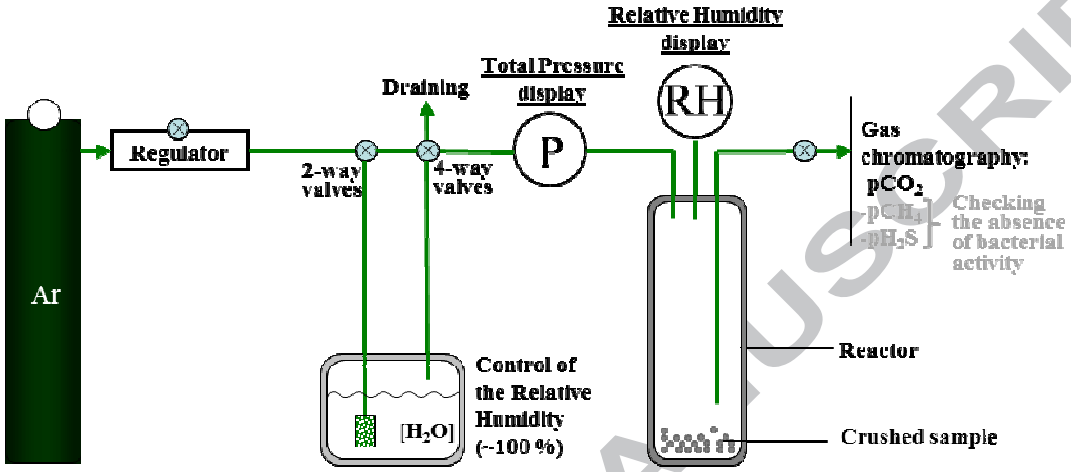

Figure 2

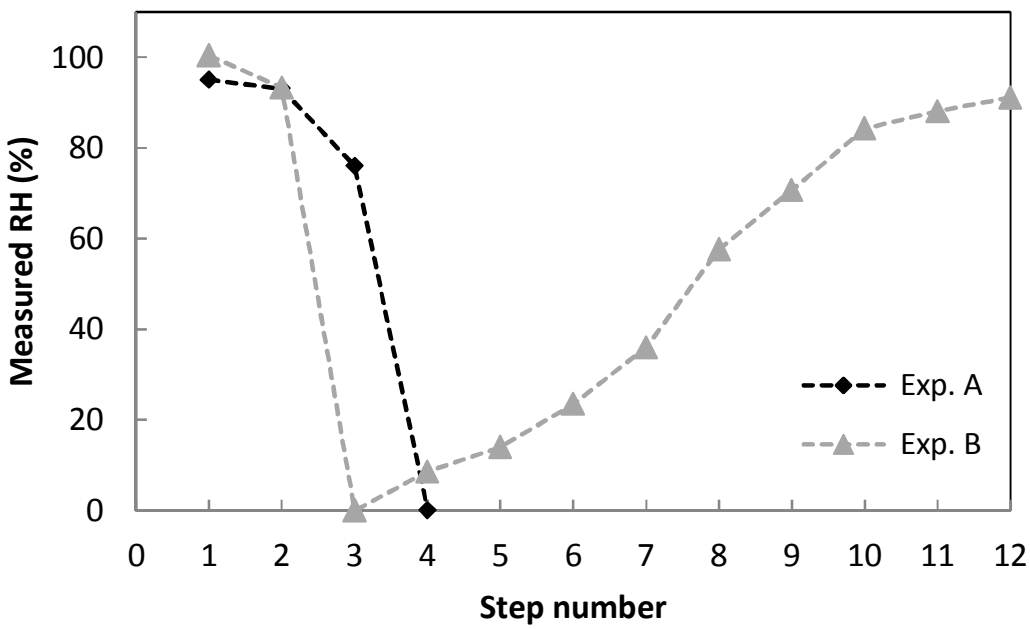

Figure 3

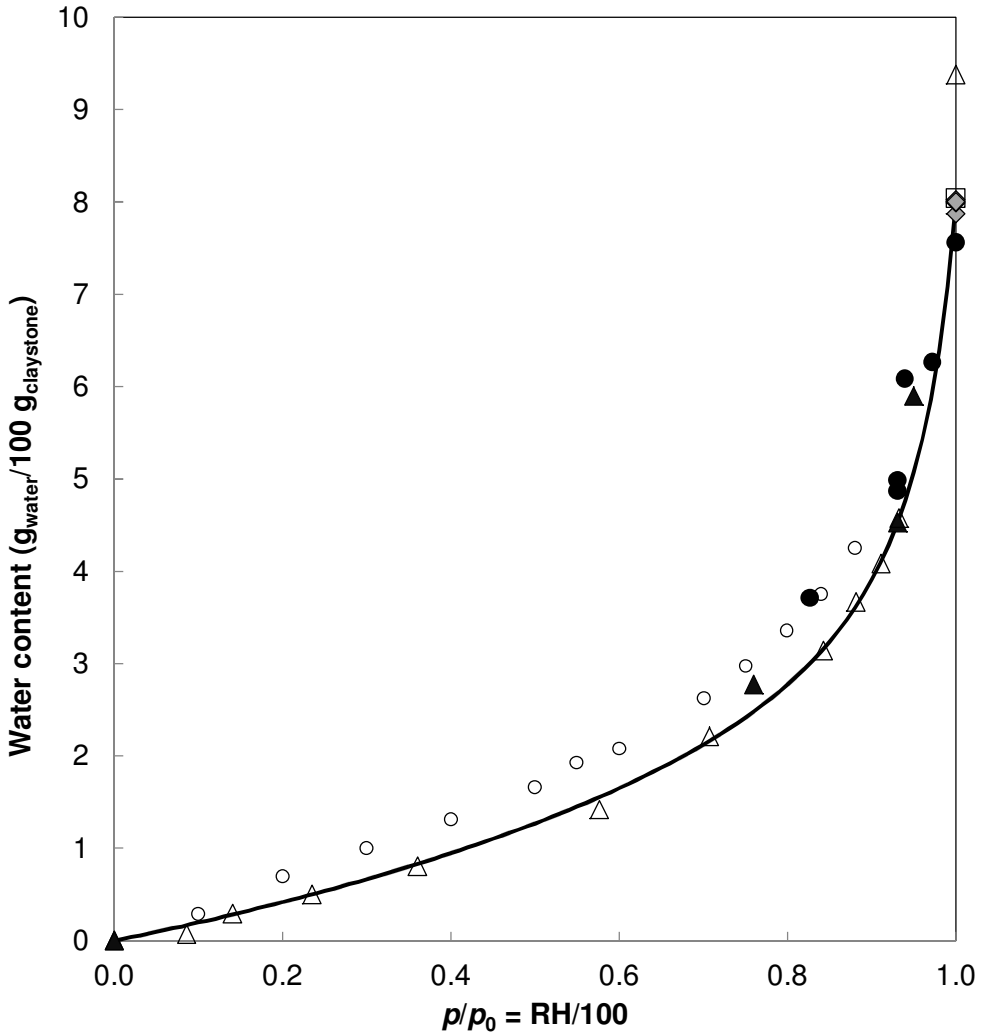

Figure 4

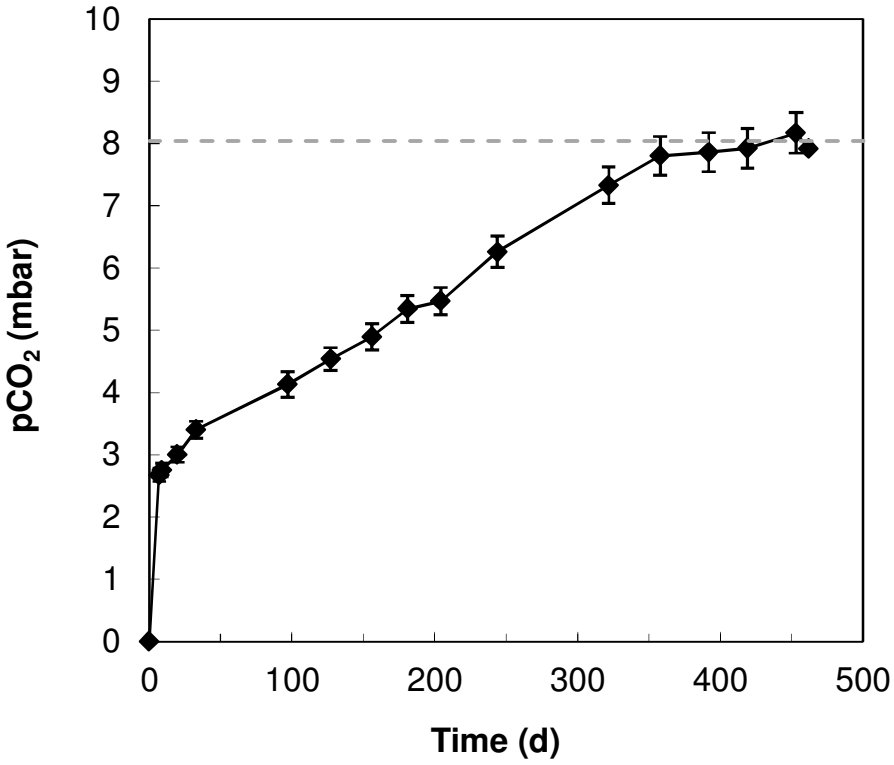

Figure 5

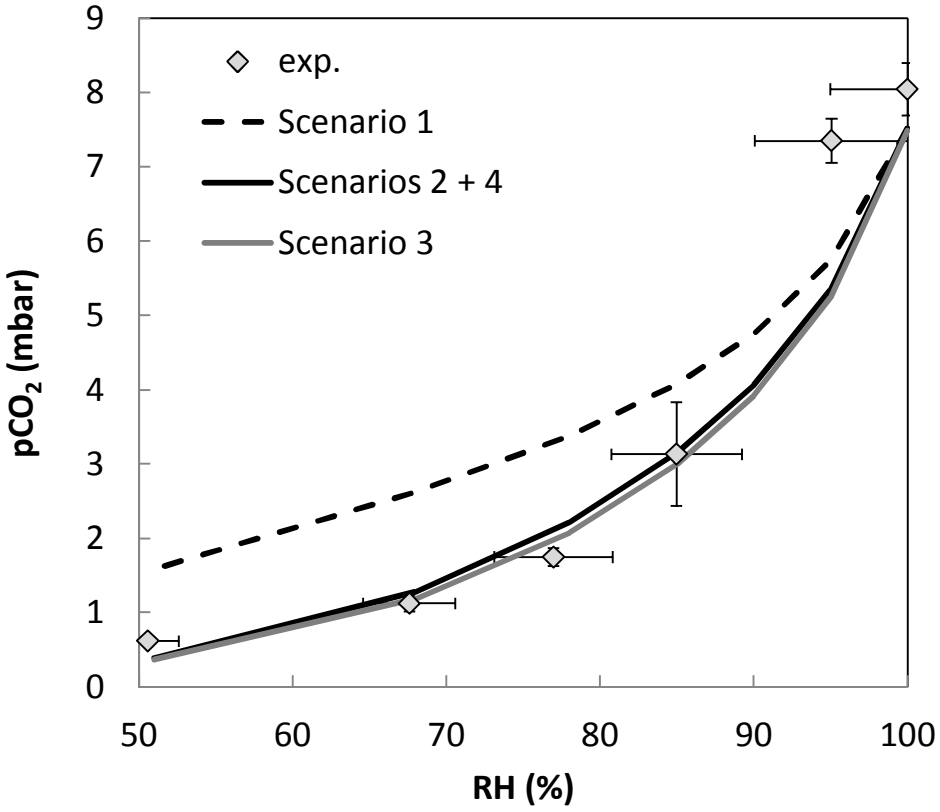

Lassin et al. (2016) "Equilibrium partial pressure of CO_2 in Callovian-Oxfordian argillite as a function of relative humidity: experiments and modelling"

Tables

Table 7: Main characteristics of the alternative model #1 of Gaucher et al. (2009)

Type of constraint	Constraint	Related parameters (concentrations)
Cation exchanger	Initial composition after cobalt hexamine method	Na, K, Ca, Mg, Sr, Fe(II)
Salt content	Leaching experiments + celestite equilibrium	Cl, S(VI)
Mineral phases at equilibrium	Quartz, calcite, pyrite, illite (imt2), chlorite (Cca-2)	Si, C, S(-II), pH, Al

Table 8: Detailed mineralogy of Sample EST10273; the total organic carbon (TOC) content and the water content correspond respectively to the mean TOC and the mean water content calculated from data acquired on samples from Unit C2b1.

Sample	EST10273
Drill hole	EST312
Lithology	C2b1
Z (NGF)	-177.49 m
Hanging wall (m)	454.71 m
	Weight (wt.%)
Mica + illite	19.0
Illite/Smectite	23.0
Kaolinite	3.5
Chlorite	2.5
Clay	**48.0**
Quartz	18.0
Feldspar	3.0
Silt	**21.0**
Calcite	23.0
Dolomite	7.0
Carbonates	**30.0**
Traces	pyrite, apatite, rutile, celestite
TOC content	0.70%
Water content	7.10%

Table 9: Experimental conditions and drying-rewetting paths (for Exp. 1) applied for determining pCO_2 as a function of RH

	Initial mass at 100% RH (g)	**Gas volume (L)**	**Initial pCO_2 (mbar)**	**Measured RH (%)**			
Exp. 1	202.3	1.2	0	95	51	68	77
Exp. 2	128.3	2.4	0	100			
Exp. 3	131.0	2.4	0	85			

Table 10: Experimental conditions and salts used for RH control during dehydration/hydration experiments to determine water content of the COx samples

	Path no.	RH control	Expected RH (%)	Measured RH (%)	Duration of experiment (days)	Mass (g)
Exp. A	1	Ar(g) flush	--	95.0	16	202.300
	2	Ar(g) flush	--	93.1	21	199.684
	3	Ar(g) flush	--	76.0	10	196.331
	4	Freeze drying	~0	--	4	191.036
Exp. B	1	COx pore water	100	100.4	95.0	131.012
	2	Ar(g) flush	--	93.3	7	125.258
	12	KNO_3	92	91.1	14	124.668
	11	$BaCl_2,2H_2O$	90	88.1	13	124.170
	10	KCl	85	84.3	14	123.543
	9	KI	69	70.7	7	122.426
	8	$NaBr,2H_2O$	58	57.6	5	121.476
	7	$NaI,2H_2O$	38	36.0	3	120.739
	6	$CaCl2,6H_2O$	29	23.5	4	120.376
	5	$LiCl,H_2O$	11	14.0	3	120.129
	4	$NaOH,H_2O$	6	8.6	3	119.862
	3	Freeze drying	~0	--	4	119.778

Table 11: Equilibrium pCO_2 measured as a function of RH and time required to reach thermodynamic equilibrium. The calculated pCO_2 values obtained according to the 4 different scenarios considered in this study are given for comparison

	Experimental results				Calculated pCO_2 (mbar)		
HR (%)	**HR error (%)**	**pCO_2 (mbar)**	**pCO_2 error (mbar)**	**Duration (days)**	**Scenario 1**	**Scenarios 2 & 4**	**Scenario 3**
100	5	8.0	0.36	462	7.51	7.51	7.65
95	5	7.3	0.29	146	5.74	5.35	5.36
85	4	3.1	0.70	753	4.07	3.15	3.07
77	4	1.7	0.12	760	3.38	2.21	2.12
68	3	1.1	0.12	486	2.62	1.28	1.21
51	2	0.6	0.03	193	1.59	0.39	0.38

Table 12: Fitting parameters for the water content model (eq. 12)

Fitting parameters	Best-fit value
a	1.837
b	0.864
c	3.521E-04
d	0.285
e	0.946